PENETRATION ANALYSES DUE TO PIPEWHIP LOADS

H. P. Lee

Ontario Hydro
700 University Avenue
Toronto, Ontario, Canada

ABSTRACT

A steel penetration embedded inside a concrete containment structure is analyzed using MSC/NASTRAN. Four separate loads of axial, shear, moment and torsion as generated by a postulated pipewhip accident are applied at the end flange of the penetration. For each load case, stress distribution across and along the penetration as well as the interface between the penetration and the surrounding concrete are described in details.

INTRODUCTION

This paper demonstrates a series of elastic analysis of a steel penetration embedded in concrete wall using MSC/NASTRAN(Ref.1). Four separate loads of axial, shear, moment and torsion as generated by a postulated pipewhip accident are applied at the front-end flange of the penetration. For each load case, stress distribution across and along the penetration as well as the interface between the penetration and the surrounding concrete are examined to see how each type of load being transferred by individual component. The ultimate resisting mode and the capacity for each case are also assessed.

DESCRIPTION OF THE PENETRATION

The penetration(Fig.1) is composed of a piece of 45mm thick cylindrical sleeve(367mm I.D.) stiffened by eight pieces of 25mm thick and 1,000mm long longitudinal stiffeners equally spaced around the sleeve. At each end of the longitudinal stiffeners, the sleeve and the longitudinal stiffeners are further stiffened by a 20mm thick annular plate referred as "puddle flange". A thick flange is fully welded at each end of the sleeve to complete the integrated penetration. The flanges are flush with the concrete wall with the circumferential edge of the front-end flange sealed and hence is not in directed contact with the concrete.

The sleeve is made of ASTM A106, Type S, Gr. B, Schedule 160 with ANSI Class 600 steel pipe flanges. The longitudinal stiffeners and puddle flanges are Canadian steel CSA G40.21M 300W. The concrete has an unconfined compressive strength(f'_c) of 3,600 psi.

FINITE ELEMENT MODEL

Figs.2 and 3 present two cross-section views of the modelled penetration and its surrounding concrete. The sleeve, longitudinal stiffeners and puddle flanges are modelled by quadrilateral plate elements while the flanges and concrete by cubic and pentagonal solids. At the intersection of sleeve and flanges where plate elements meet solid elements, physical continuity during deformation is achieved by specifying displacement compatible relationships. Note that double nodes are provided to disconnect the concrete from the sealed steel flange.

Concrete wall support is 'fixed' at 3000mm from the centre of the penetration which is judged adequately far enough so that the boundary condition will not affect the resulting stress in the penetration.

Only a quarter of the penetration/concrete system is actually modelled and analyzed by providing appropriate boundary conditions to reflect the symmetrical or anti-symmetrical conditions for different load cases.

LOADS

Fig. 4 shows how a mechanical pipe is connected to the front-end flange of the penetration through a flue head which is assumed to be rigid. Four different loads are applied as follows:

Case 1. Axial force	=	13,000 kN
Case 2. Shear force	=	7,800 kN
Case 3. Bending moment	=	1,036 kN-m
Case 4. Torsion	=	1,183 kN-m

The orientation of these loads are schematically shown in Fig.5. These loads are treated individually so that the modes of transferring stress for different types of load can be examined. These loads are converted to nodal forces applied at the flue head-flange intersection (see location 'A' in Fig.4)

RESULTS AND DISCUSSIONS

I. Stress in Penetration

Among the four loading cases, the Case 1 under axial force generates the highest stresses in penetration. However these stresses are significant only at the front-end flange which is directly under the applied load(Fig.6). The stresses attenuated rapidly to the adjacent areas resulting in smaller stress in sleeve, longitudinal stiffeners and puddle flanges.

Stresses in the longitudinal stiffeners are primarily transferred from the sleeve. The stresses transferred from the surrounding concrete to the longitudinal stiffeners through friction are less significant.

The low stresses in the puddle flange indicate that it did not play an important role in resisting the applied load through direct interaction with surrounding concrete. The major function of the puddle flange lies to stiffen the sleeve and longitudinal stiffeners.

The stresses in the rear-end flange are minimum and negligible.

II. Stresses at Penetration/Concrete Interfaces

Stresses are transferred from the penetration to the surrounding concrete through their interface by bonding(tensile and/or shear) and bearing(compression). Table 1 summarizes the percentage of the applied load being resisted by different interfaces between concrete and individual penetration component.

In **Case 1**, Fig.7 shows the direct tensile stress in concrete immediately behind the flange. It indicates that the stresses at interface (Section X) are higher but decay more quickly toward the boundary along the radial direction than the stresses at location farther behind (Section Y and Z). Two types of concrete tensile strength, the direct tensile strength (f_t) and the modulus of rupture(f_r), are identified for comparison. The bond between the flange and concrete will be destroyed as expected.

The longitudinal shear stress at sleeve/concrete interface is shown in Fig.8. Note that the shear stress in the front-end flange portion is actually decreased (solid line in the figure) because the stress in this area is dominated by the direct tension as discussed above. Concrete shear strength (v_c) and concrete/steel friction strength (v_f) are also plotted for comparison. It can be seen that the bond between the concrete and the sleeve will be diminished along the front half of the sleeve.

In **Case 2**, the major portion of the shear force is transferred from the flange directly to the concrete behind the flange through radial and tangential shear stress components. For the radial component, the maximum stress occurs at $q=90^{o}$ as shown in Fig. 10 and 11. The other component of tangential shear stress with the maximum at $q=0^{o}$ is shown in Fig. 12 and 13. Both stress components exceed the allowable shear strength.

The main stress transferred from the sleeve to its surrounding concrete is the radial normal bearing stress(see Fig.9). It has the maximum in compression at $q=90^{o}$ and in tension at $q=270^{o}$. Eventually, the tensile side stress will exceed the allowable and the corresponding force will be passed to the

compression side. This compressive normal stress is reflecting the phenomenon of "concrete wedge" due to shear for embedded parts.

In **Case 3**, stresses transferred from the flange to the concrete behind are similar to that of the axial load case. However, the stresses in the present case are smaller and are anti-symmetrical with respect to the neutral axis while the previous case is symmetrical. Figs.14 and 15 describe the longitudinal normal stress which indicates that, even though the compressive side stress is below f'_c, the tensile side stress exceeds the allowable. Interface bond in tension will be deteriorated.

In **Case 4**, the most important stress from flange to concrete is the tangential shear stress t_{zq} (Figs. 16 and 17). This stress carried the major portion of the total torque through friction between the concrete and the flange and also exceeds the allowable. The remaining portion of the torque is transferred from sleeve to concrete also through friction shear at the interface.

III. Stress in Concrete

It has been shown in the previous figures that high tensile and shear stresses in concrete concentrate in the vicinity immediately behind the flange and gradually reduce toward remote areas.

Fig.18 presents a vectorial plot for Case 1 identifying the magnitude and orientation of the direct tensile stress. A "truss action" is observed in that the axial load is carried by two components shown as dotted lines in the figure. One component is carried by steel directly from flange to sleeve and the other component by concrete. The component carried by concrete is not uniformly distributed behind the flange. Higher stresses are directed towards the corner marked as 'B' in the figure. The tendency of higher stress and orientation toward the point B indicates a stress concentration in that area due to the gap between concrete and the circumferential edge of the flange, and hence created a corner of discontinuity.

Another important concrete stress around the penetration is the tangential shear stress, t_{qz}, occurred in Case 3 (Fig. 19). Note that this is the horizontal shear stress within concrete (not on the interface between concrete and penetration) with the maximum at the plane of the neutral axis. It is the horizontal (longitudinal) shearing stress generated due to bending of the penetration/concrete equivalent beam system. This stress is associated with the above discussed longitudinal normal stress s_z(Fig.15) and hence is significant at the front end of the penetration.

IV. Assessment of Ultimate Resistance

As noted, the concrete strength through tension and shear at steel interface will be exceeded at the front-end portion of the penetration. Consequently, the stiffness in tension and shear are ignored and the entire load is assumed to be resisted solely by concrete in compression. Assuming that the bearing stress distribution pattern does not change, the final stresses are extrapolated from the analyses and compared with material strength.

Case 1: Axial Force

Failure in concrete/flange tensile bond will cause the entire axial load being transferred from the flange to the sleeve. Dividing the total load by the sleeve cross-sectional area results in a tensile stress of 223 MPa and is below yielding (0.9 f_y).

Transferring the increased stress from the sleeve to the surrounding concrete results in the increased shear stress approximated by the dotted line in Fig.8. A progressive deterioration of shear friction bond between concrete and sleeve will occur starting from the front end toward the rear. Similarly, a progressive deterioration of longitudinal stiffener/concrete interface shear-friction bond is also likely to occur.

Having failed in shear mode, the applied load will eventually be transferred to the rear-end flange which functions as a mechanical anchor. The entire load is now carried from this anchor head to the concrete and the integrity of the penetration/concrete system will rely on its pull-out strength.

The penetration is embedded across the entire thickness of the wall. Several studies(Refs. 2 to 5) including linear and nonlinear finite element analyses for shallow embedded anchor bolt indicates that the pull-out failure involves the development of a shear cone. It is judged to be conservative to extend similar conclusion to the present case because the deeply embedded part will generate less severe local stress and spread the load into a much larger area. A 45^{o} shear cone is therefore postulated and the strength is compared with various design codes(e.g. Ref.6) and is found adequate.

Case 2: Shear Force

Failure in concrete/flange shear bond will cause the entire shear force being transferred from the flange to the sleeve. The resulting maximum shear stress at the sleeve section is found to be 117 MPa (0.5 f_y).

The next resisting phase will be the sleeve and its surrounding concrete subjected to the radial normal stress at interface. The integrity of the penetration/concrete system will have to rely on this interface bearing which is assessed using the following two approaches:

Evaluation by Proportioning up the Elastic Stress

Assuming the entire shear force to be resisted by this bearing mode, the maximum stress(at $q=90^{o}$) is shown in Figs.20 and 21 by extrapolating from the elastic results and is approximately 5 f'_c. This approach is judged to be conservative and the value may be treated as the upper bound.

Evaluation Based on Beam on Elastic Foundation

An alternative evaluation of this bearing stress is treating the penetration/concrete interaction as a finite beam on Winkler's elastic foundation subjected to an applied load at one end. For this purpose, the coefficient of subgrade(concrete) reaction, K, is conservatively estimated to be 34.6×10^6 kN/m^3 by using the Young's modulus and Poisson's ratio based on the theoretical formulation in Ref. 7. Even though the exact K value is not known, the result is not expected to be affected significantly as a difference of 100 to 200 percent in K may change the structural element behaviour only by 15 to 25 percent(Ref.8).

Calculation is then conducted using the mathematical expression from Ref.9. Results are then compared with that through interpolation of graphic representation in Ref. 10 and are found in good agreement. The maximum is around 3.4 f'_c and is shown in Figs.21 and 22. It is judged that this 3.4 f'_c maximum bearing stress is a more realistic value than the 5 f'_c by proportioning up the elastic analysis results and is acceptable in a confined condition.

Case 3: Bending Moment

Local tensile failure at the flange/concrete interface and subsequent shear failure of concrete around the sleeve are likely to occur. Transfer of entire moment from the flange to the sleeve result in the maximum

fibre stress of 82 MPa (0.35 f_y) in steel. The final moment resistance will rely on the normal bearing stress between the concrete and the steel penetration similar to the previous shear load case. An evaluation following the same procedure is conducted except that in the present case a bending moment is applied at one end of the beam on elastic foundation. Assuming that the entire moment is carried by this bearing mode, the resulting maximum bearing stress is approximately equal to f'_c as shown in Figs.22 and 23 and is much less critical.

Case 4: Torsion

Failure of interface bond between flange and concrete results in the total torque being passed to the sleeve. The maximum shear stress in sleeve due to transfer of torque from flange is found to be 108 MPa (0.45 f_y).

The torque is then transmitted from sleeve to its surrounding concrete. The shear friction strength at the sleeve/concrete interface is unlikely to be able to hold the entire torque. The torque has to be transmitted to the longitudinal stiffeners and eventually arrested through bearing between the longitudinal stiffeners and their surrounding concrete.

Fig.24 illustrates the bearing stress along the radial direction. It can be seen that stresses actually decrease toward the stiffener/sleeve intersection (solid line in the figure). This is because that significant stresses are taken through shear friction at concrete/sleeve interface which was considered effective in the elastic analysis. Eventually, this interface shear friction will fail and result in the bearing stress distribution shown as dotted lines in the figure.

The bearing stress along the longitudinal direction of stiffener/concrete interface is shown in Fig.25. Similarly, stresses decrease at the front-end portion of the stiffener (solid line in the figure) in the elastic analysis because that the torque is shared by transmitting firstly from the sleeve to the puddle flange and then from the puddle flange to the concrete through shear friction at their interfaces. Hence the torque is not entirely transferred from the sleeve to the concrete directly. With a similar assumption of shear bond failure at the puddle flange/concrete interface, the resulting stress distribution is shown as dotted line in the figure.

Since concrete is not effective in tensile stress which was fully accounted in elastic analysis. A more realistic stress distribution is postulated by shifting the elastic distribution curve toward the compression side until the bearing stress at the tensile side becomes zero. The resulting maximum bearing stress in such a confined condition is about $1.75f'_c$ as shown in Figs.24 and 25.

CONCLUSION

A penetration subjected to four separate loads of axial, shear, moment and torsion has been analyzed using MSC/NASTRAN. The maximum stress is localized in a small area in a confined condition.
High stresses in tensile and shear eventually will fail the interface bond between flange/concrete and sleeve/concrete. The final arrest of the loads relies on the bearing mode of resistance between the concrete and the penetration. The ultimate bearing stress for all these cases are evaluated based on conservative assumptions and the highest bearing stress of $3.4f'_c$ is generated due to the shear load.

These linear analyses are to provide insight on the stress distribution pattern, possible failure modes and alternate ultimate load carrying mechanism. For further detailed investigation on the ultimate penetration/concrete coupled response, a nonlinear analysis is recommended.

REFERENCES

(1) MSC/NASTRAN User's Manual, Version 66, The MacNeal-Schwendler Corporation, Los Angeles, Califorina, USA, November 1988.
(2) The, R.E. and Mendonca, J.A., "Tensile Capacity of Short Anchor Bolts and Welded Studs: A Literature Review", ACI Journal, July/August, 1982.
(3) Stone, W.C. and Carino, N.J., "Deformation and Failure in Large-Scale Pullout Tests", ACI Journal, November/December, 1983.
(4) Stone, W.C. and Carino, N.J., "Comparison of Analytical With Experimental Internal Strain Distribution for Pullout Test", ACI Journal, January/February, 1984.
(5) Ottesen, N.S., "Nonlinear Finite Element Analysis of Pullout Test", Journal of Structural Division, ASCE, Vol. 107, No. St4, April, 1981.
(6) PCI Design Handbook - Precast Prestressed Concrete, 3nd ed., Prestressed Concrete Institute, Chicago, 1985.
(7) Vesic, A.B., "Bending of Beams Resting on Isotropic Elastic Solid", Proceedings of ASCE, Vol. 87, No. EM2, April, 1961.
(8) Bowles, J.E., "Foundation Analysis and Design", 2nd ed., Mcgraw-Hill, 1977.
(9) Roark, R.J. and Young, W.C., "Formulas for Stress and Strain", 5th ed., Mcgraw-Hill, 1975.
(10) Seely, F.B. and Smith, J.O., "Advanced Mechanics of Materials", 3rd ed., Toppan Co., 1983.

TABLE 1: MODES OF RESISTANCE AGAINST THE APPLIED LOADS

	LOAD CASE	1	2	3	4
INTERFACE	LOAD TYPE	Axial	Shear	Moment	Torsion
RESISTANCE	MAGNITUDE	13,000 kN	7,800 kN	1,036 kN-m	1,183 kN-m
Between concrete and front-end flange		54%	77%	65%	79%
Between concrete and sleeve		27%	11%	28%	13%
Between concrete and longitudinal stiffeners		15%	2%	1.5%	1%
Between concrete and front-end puddle flange		2%	2%	0.5%	2%
Miscellaneous		2%	8%	5%	5%

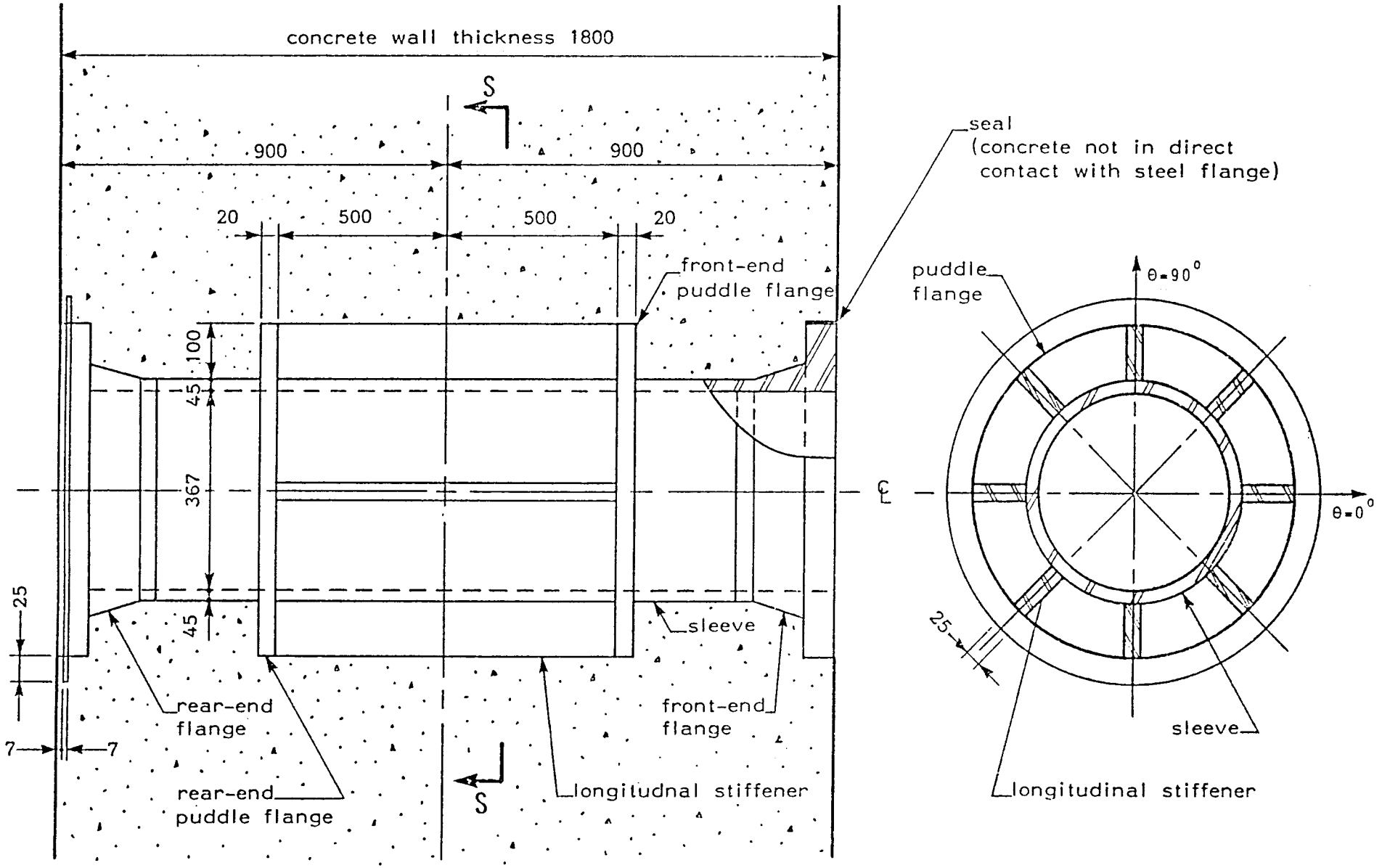

(a) Longitudinal View

(b) Section S

FIG. 1: GEOMETRY OF PENETRATION

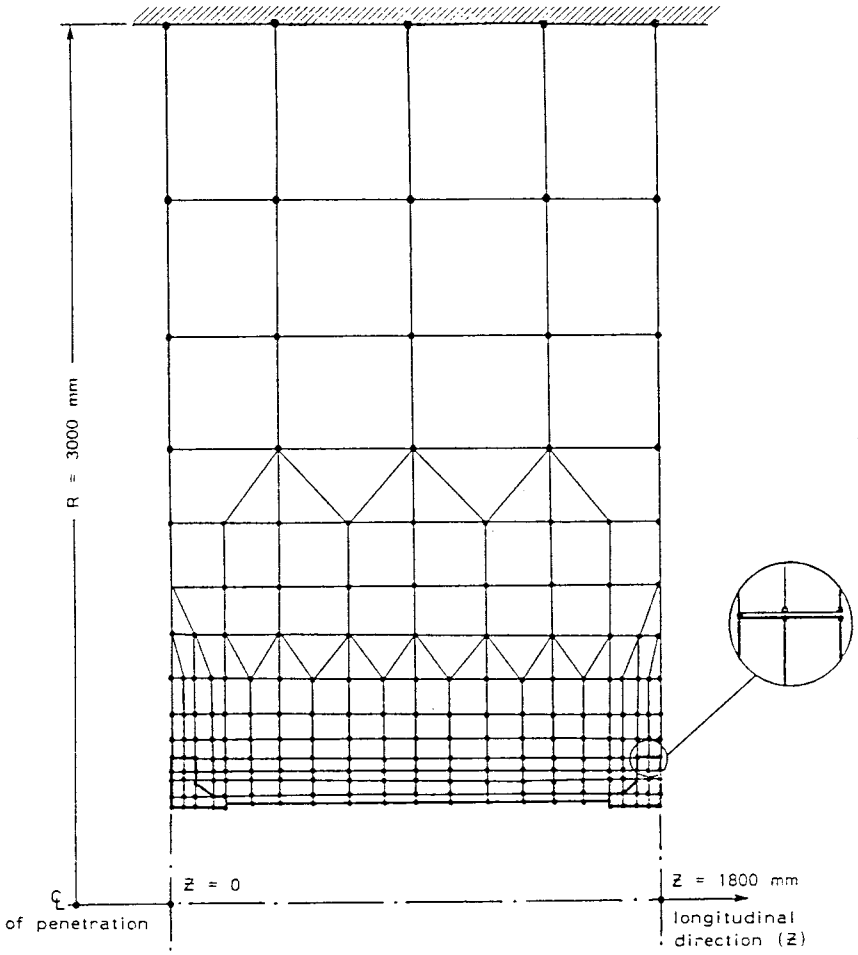

FIG. 2: FINITE ELEMENT MODEL (Longitudinal View)

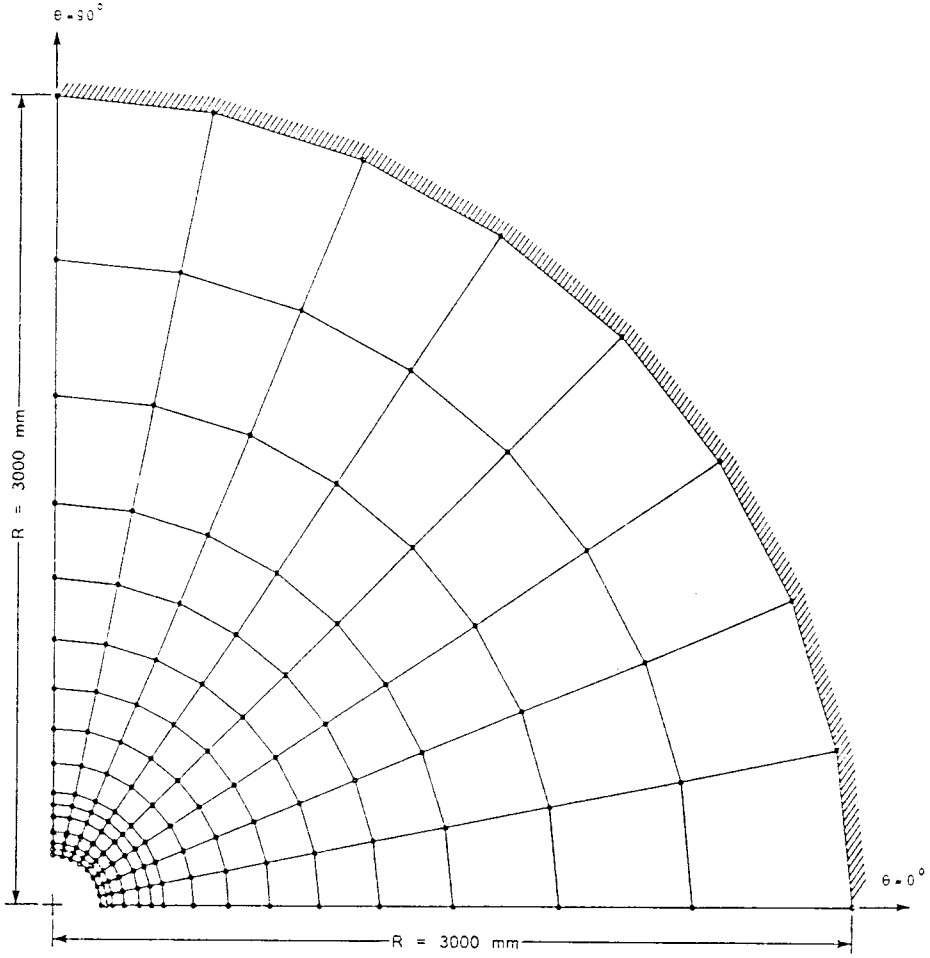

FIG. 3: FINITE ELEMENT MODEL (Cross-Section View)

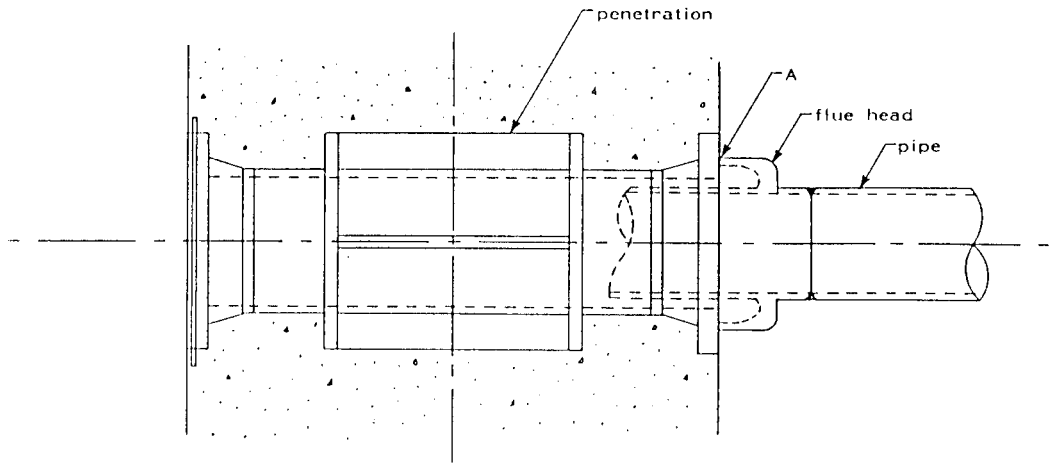

FIG. 4: PIPE-PRNETRATION CONNECTION

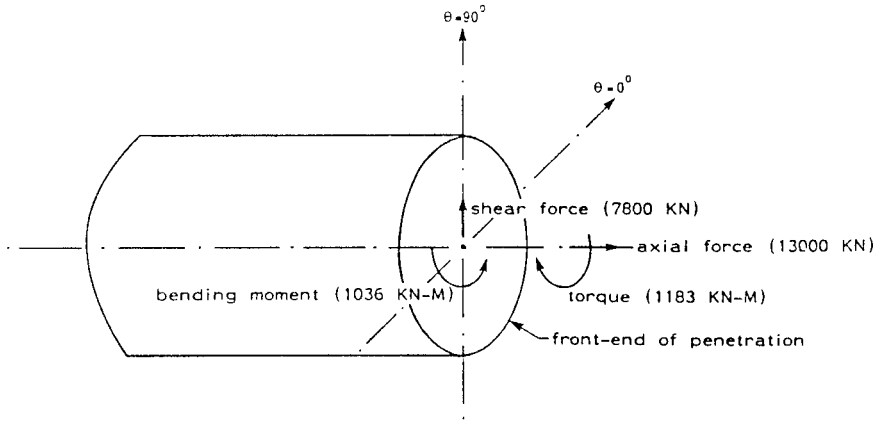

FIG. 5: ORIENTATION OF THE APPLIED LOADS

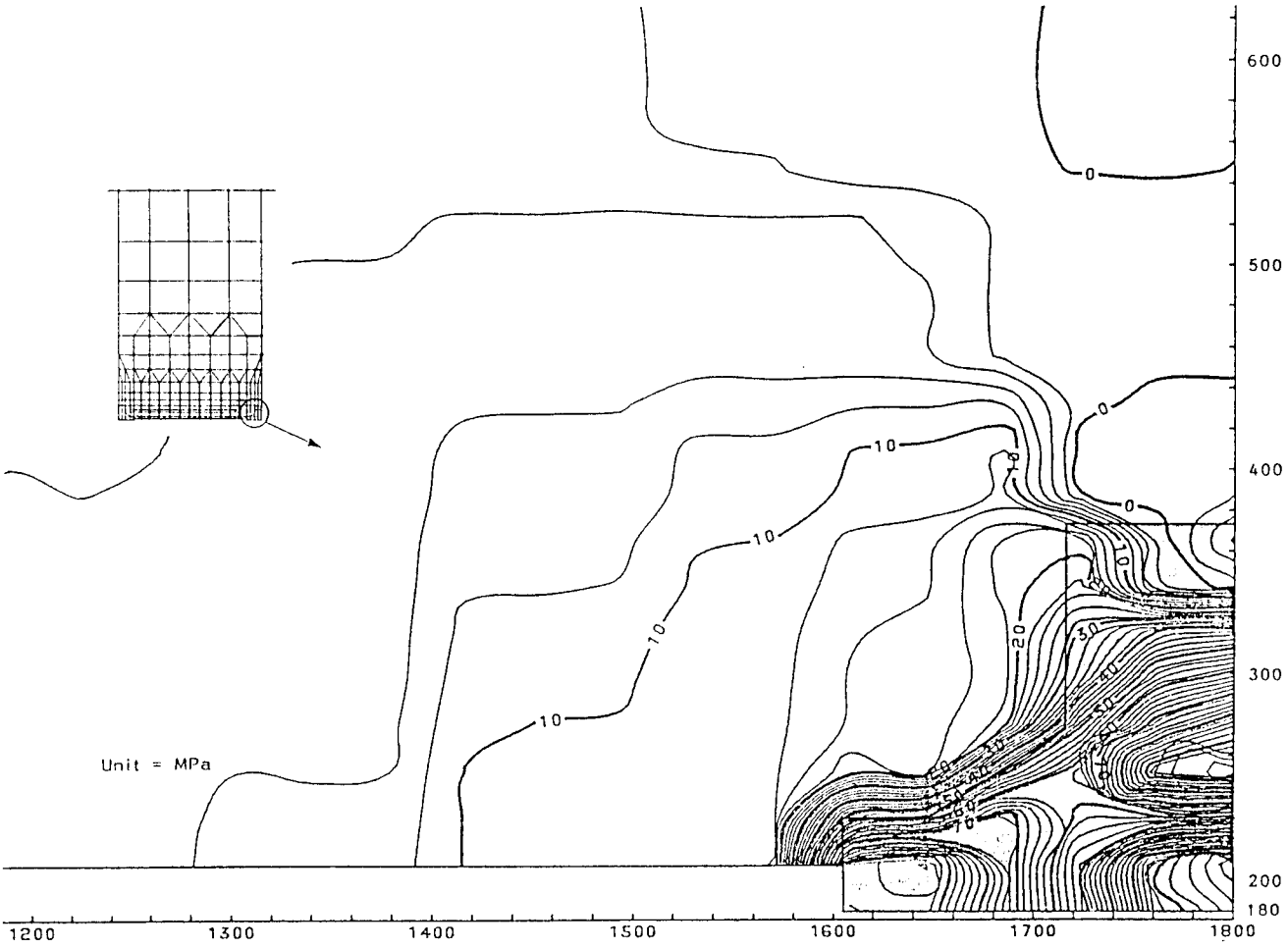

FIG. 6: CONTOUR OF LONGITUDINAL NORMAL STRESS (σ_z)
LOAD CASE 1 = AXIAL FORCE

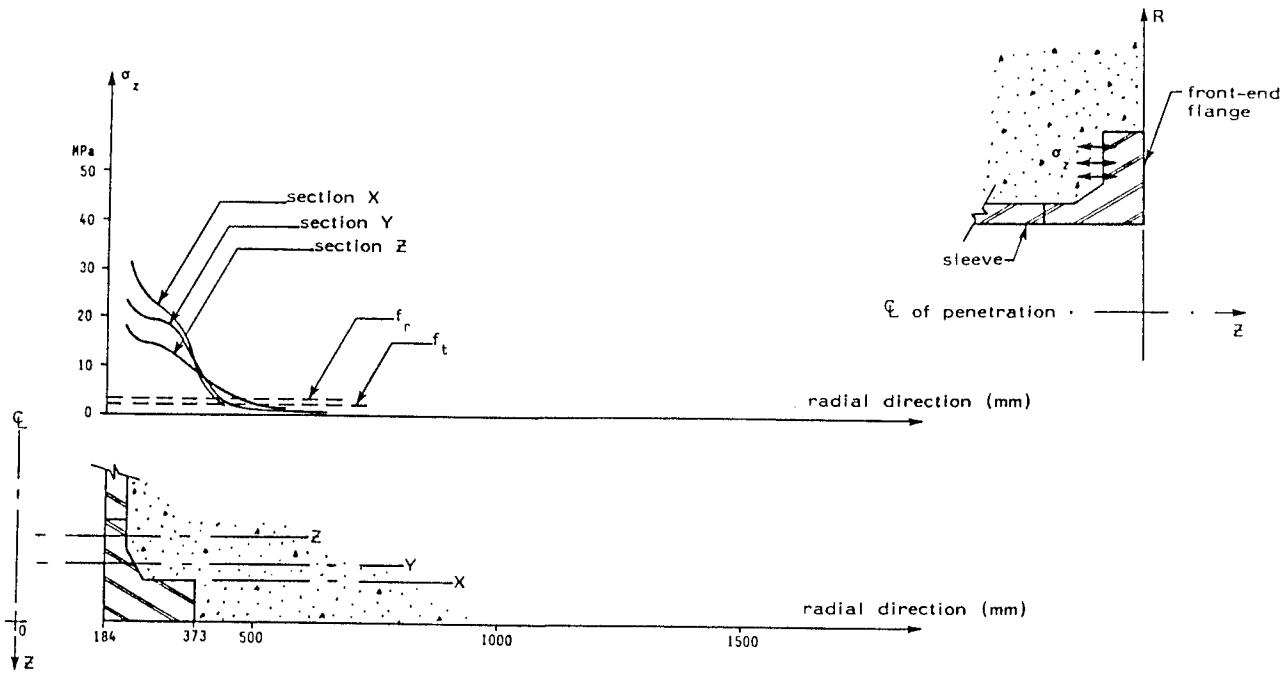

FIG. 7: LONGITUDINAL TENSILE STRESS (σ_z) OF CONCRETE BEHIND THE FLANGE
LOAD CASE 1 = AXIAL FORCE

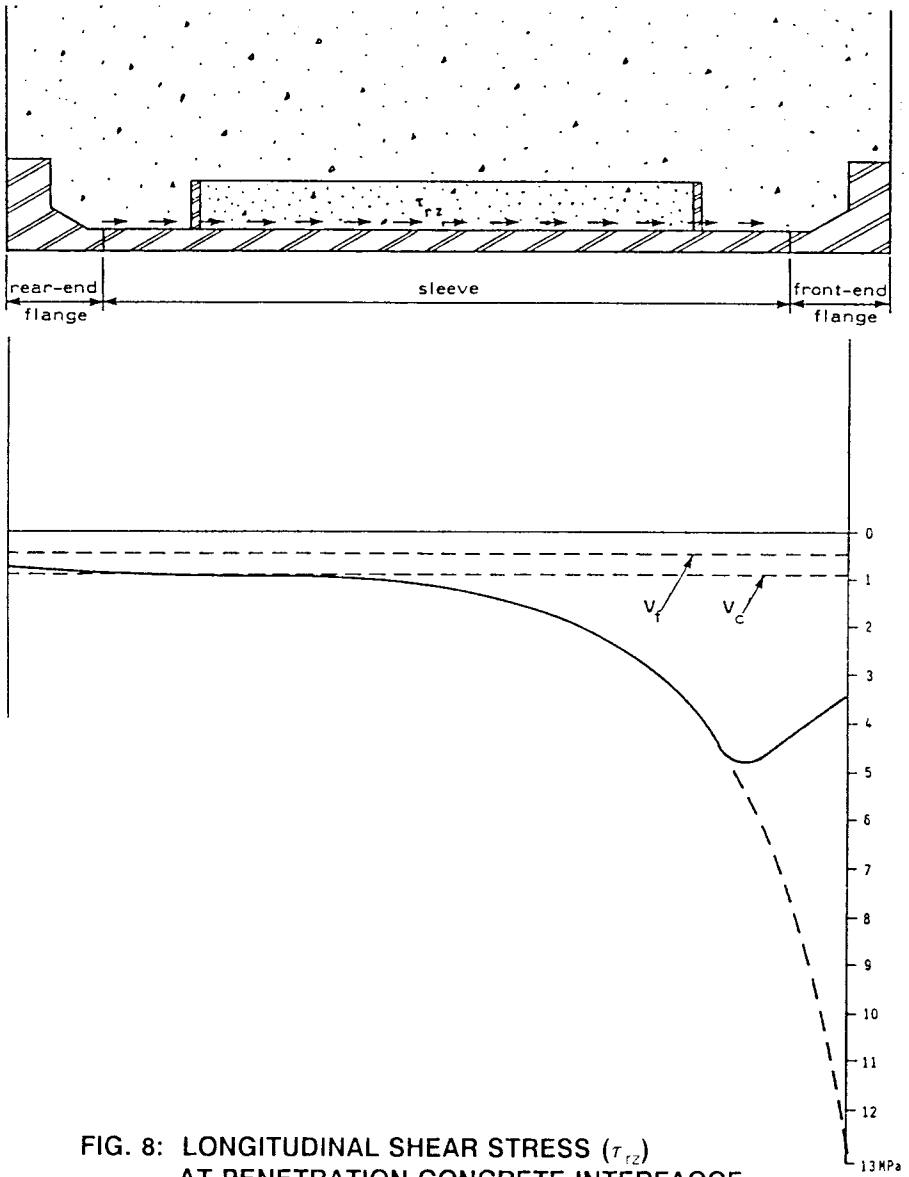

FIG. 8: LONGITUDINAL SHEAR STRESS (τ_{rz})
AT PENETRATION-CONCRETE INTERFACCE
LOAD CASE 1 = AXIAL FORCE

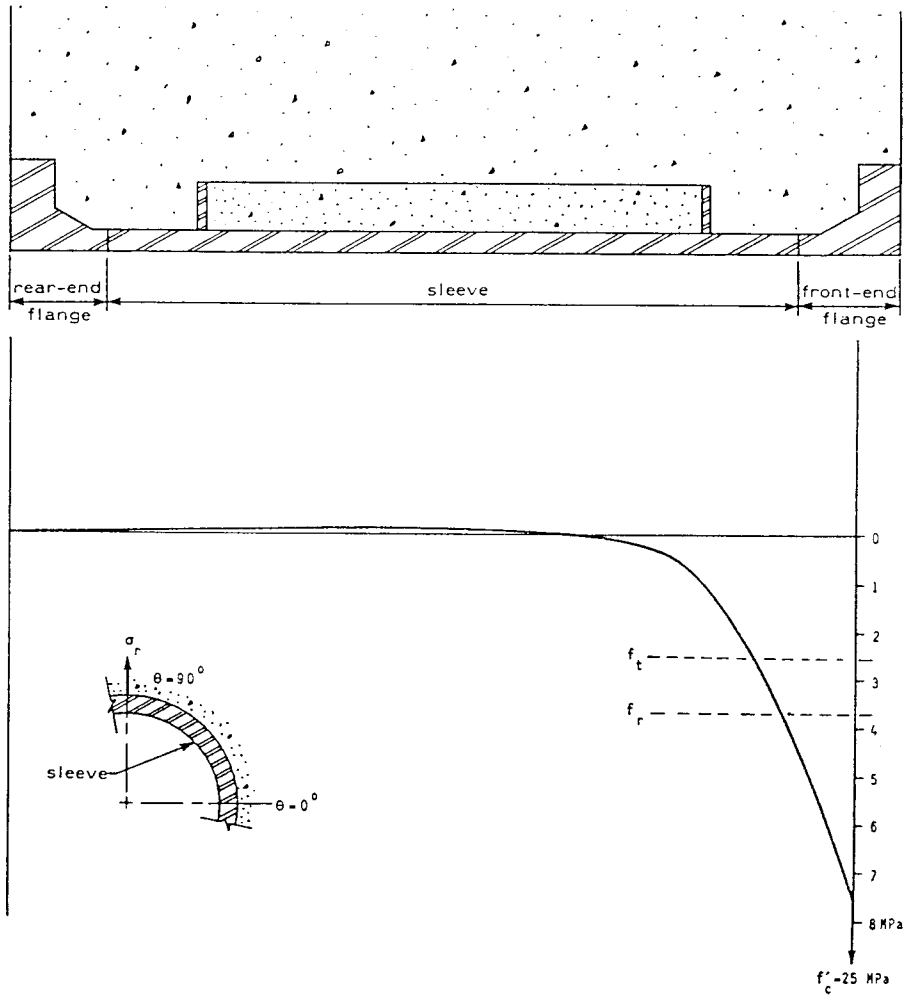

FIG. 9: RADIAL NORMAL STRESS (σ_r) OF CONCRETE AT θ = 90°
LOAD CASE 2 = SHEAR FORCE

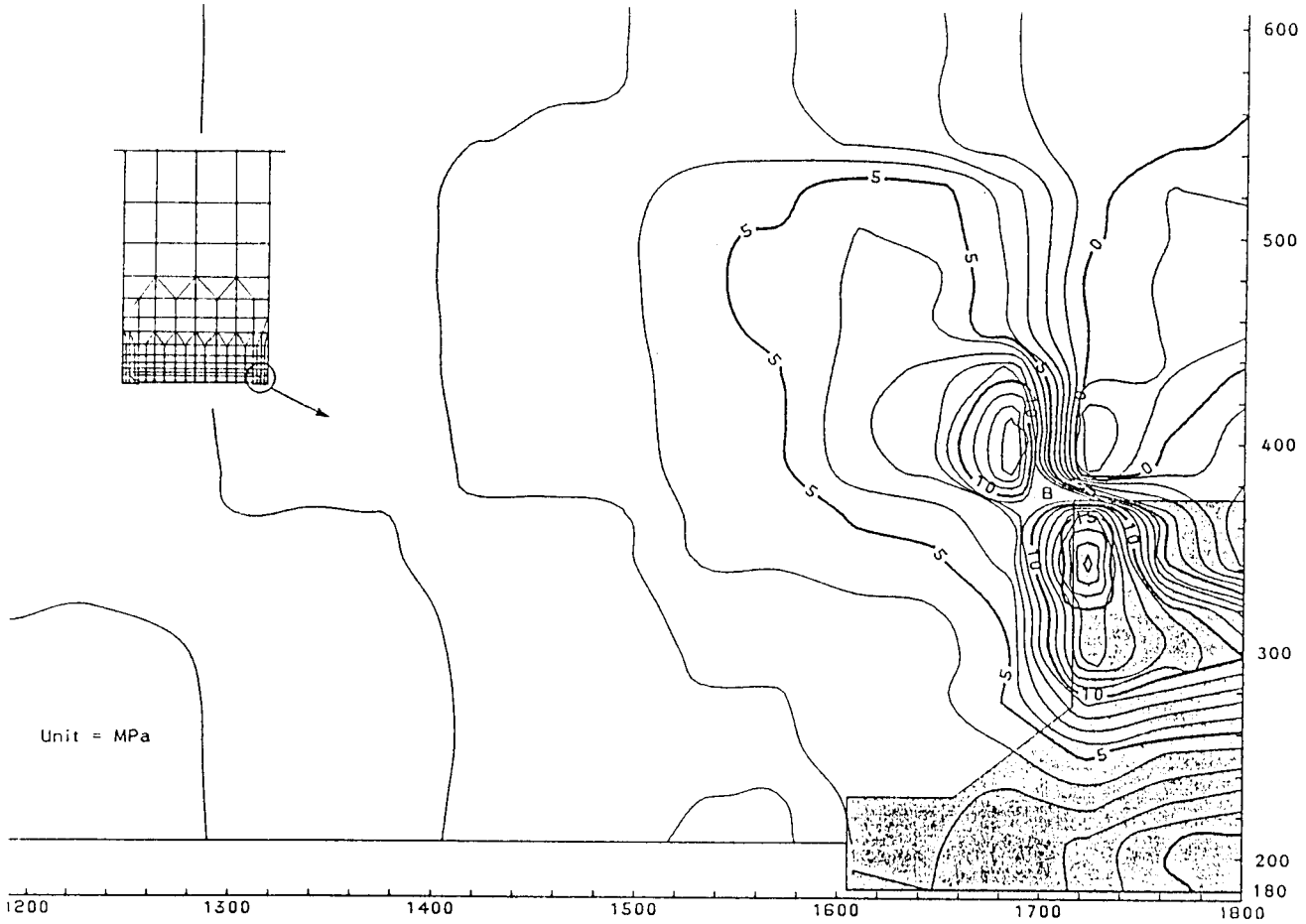

FIG. 10: CONTOUR OF RADIAL SHEAR STRESS (τ_{zr}) AT θ = 90°
LOAD CASE 2 = SHEAR FORCE

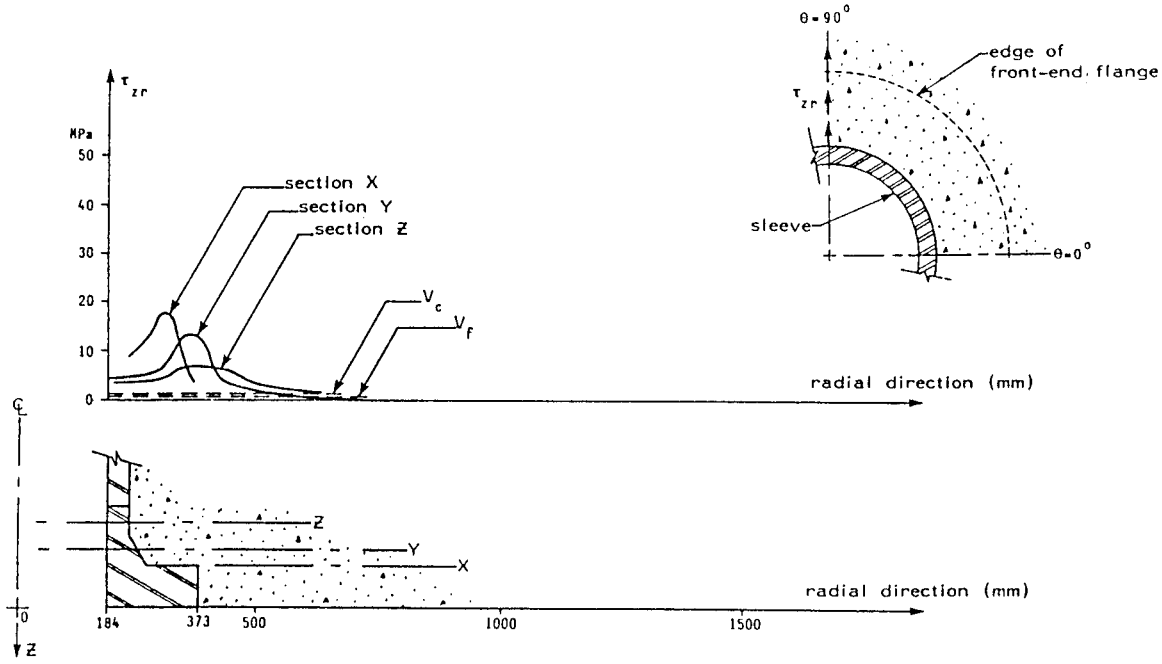

FIG. 11: RADIAL SHEAR STRESS (τ_{zr}) OF CONCRETE BEHIND THE FLANGE AT θ = 90°
LOAD CASE 2 = SHEAR FORCE

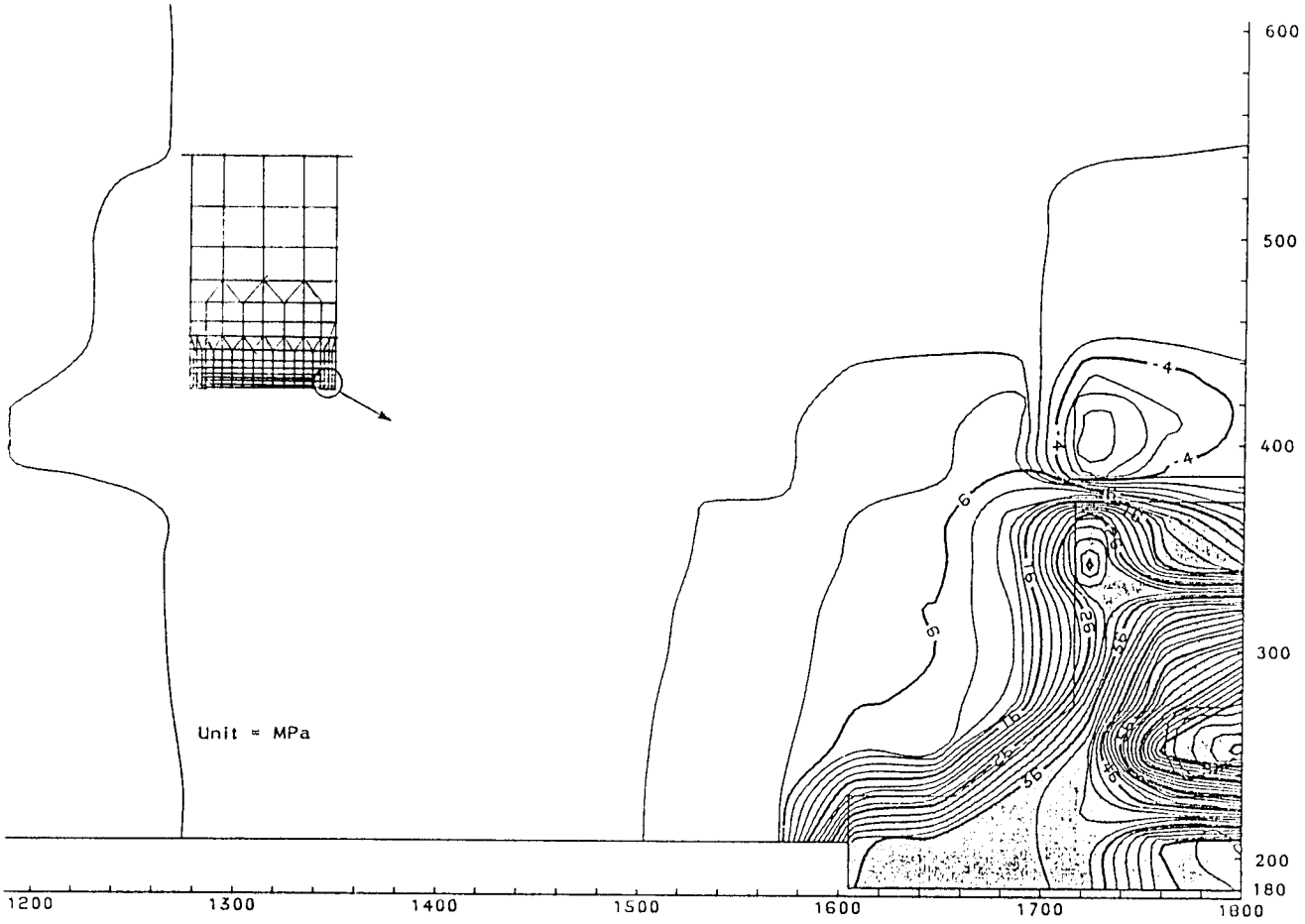

FIG. 12: CONTOUR OF TANGENTIAL SHEAR STRESS ($\tau_{z\theta}$) AT θ = 0°
LOAD CASE 2 = SHEAR FORCE

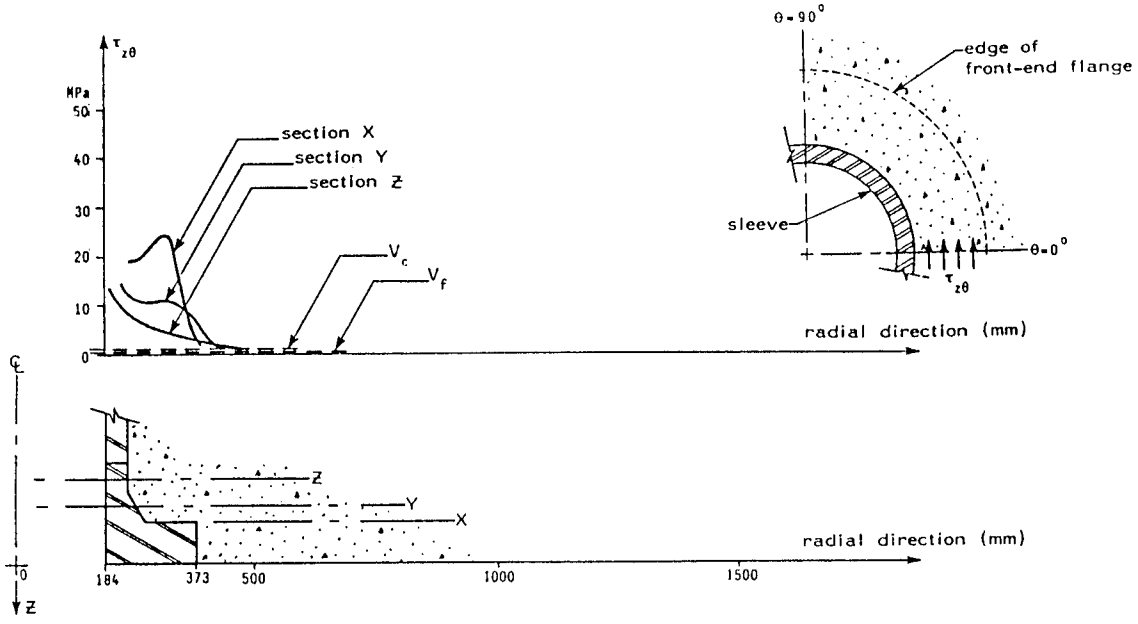

FIG. 13: TANGENTIAL SHEAR STRESS ($\tau_{z\theta}$) OF CONCRETE BEHIND THE FLANGE AT θ = 0°
LOAD CASE 2 = SHEAR FORCE

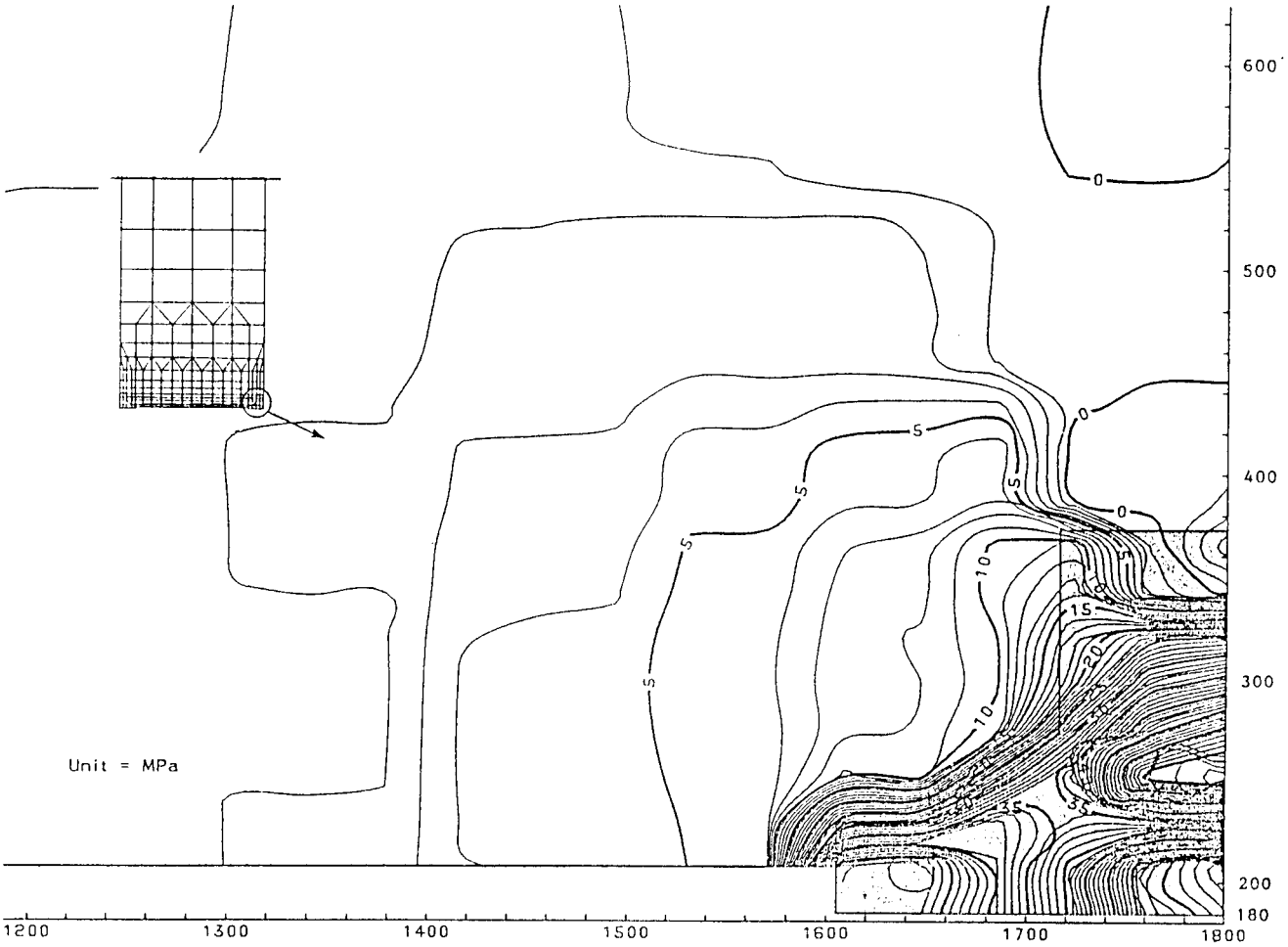

FIG. 14: CONTOUR OF LONGITUDINAL NORMAL STRESS (σ_z) AT θ = 0°
LOAD CASE 3 = BENDING MOMENT

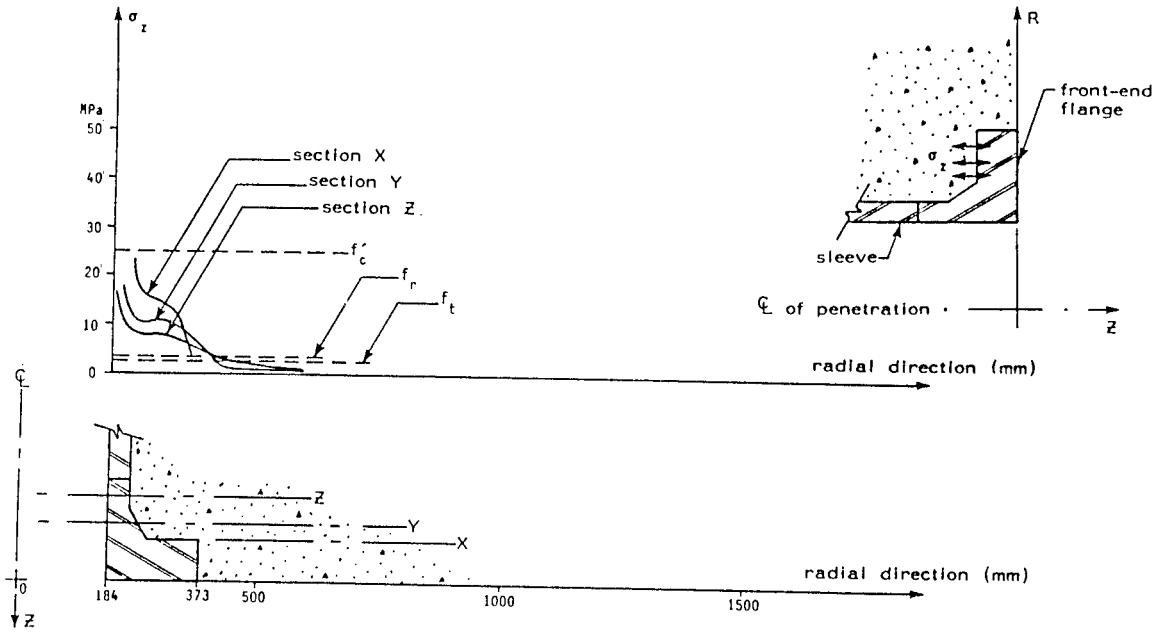

FIG. 15: LONGITUDINAL NORMAL STRESS (σ_z) OF CONCRETE BEHIND THE FLANGE AT θ = 0°
LOAD CASE 3 = BENDING MOMENT

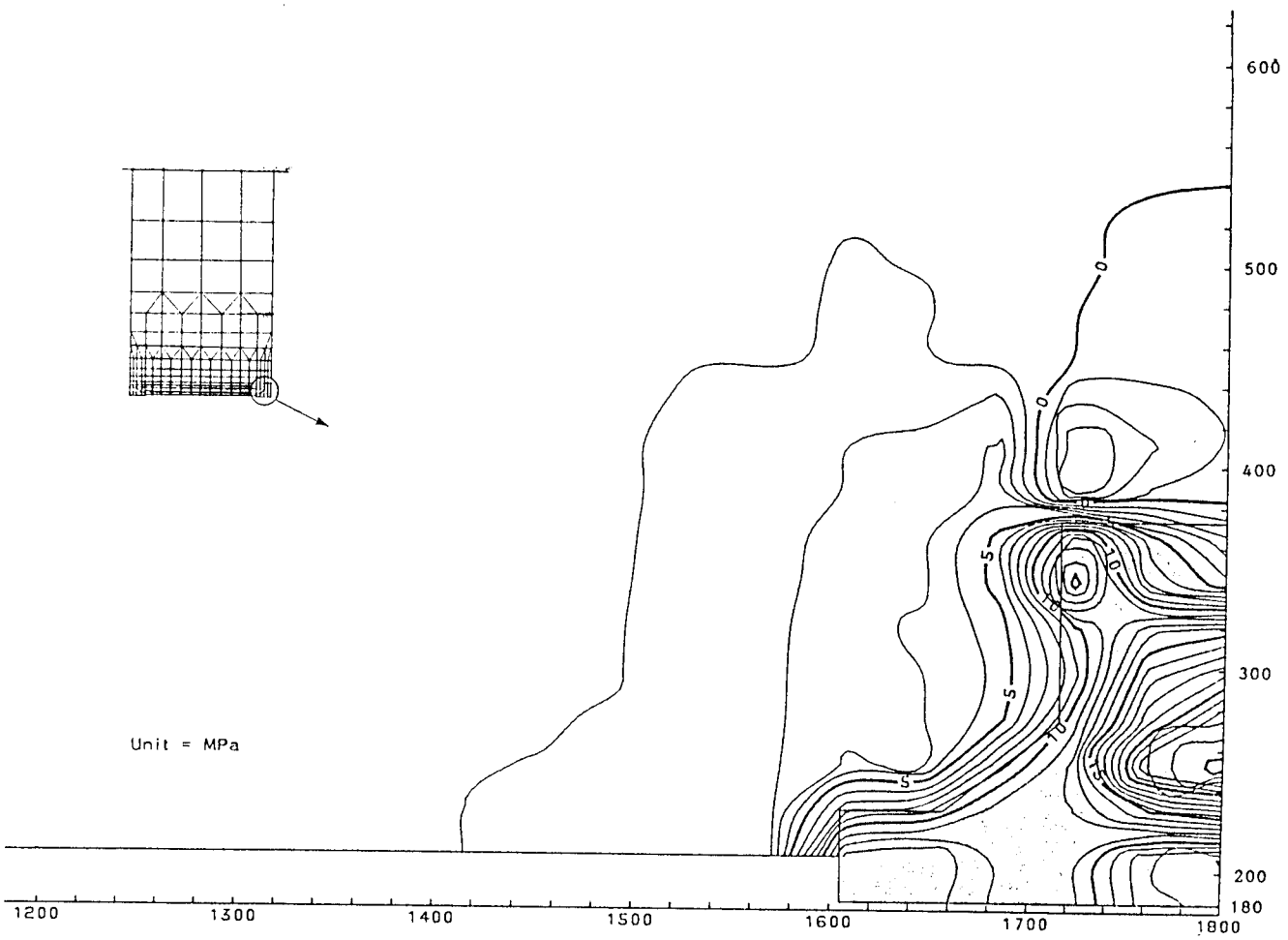

FIG. 16: CONTOUR OF TANGENTIAL SHEAR STRESS ($\tau_{z\theta}$)
LOAD CASE 4 = TORSION

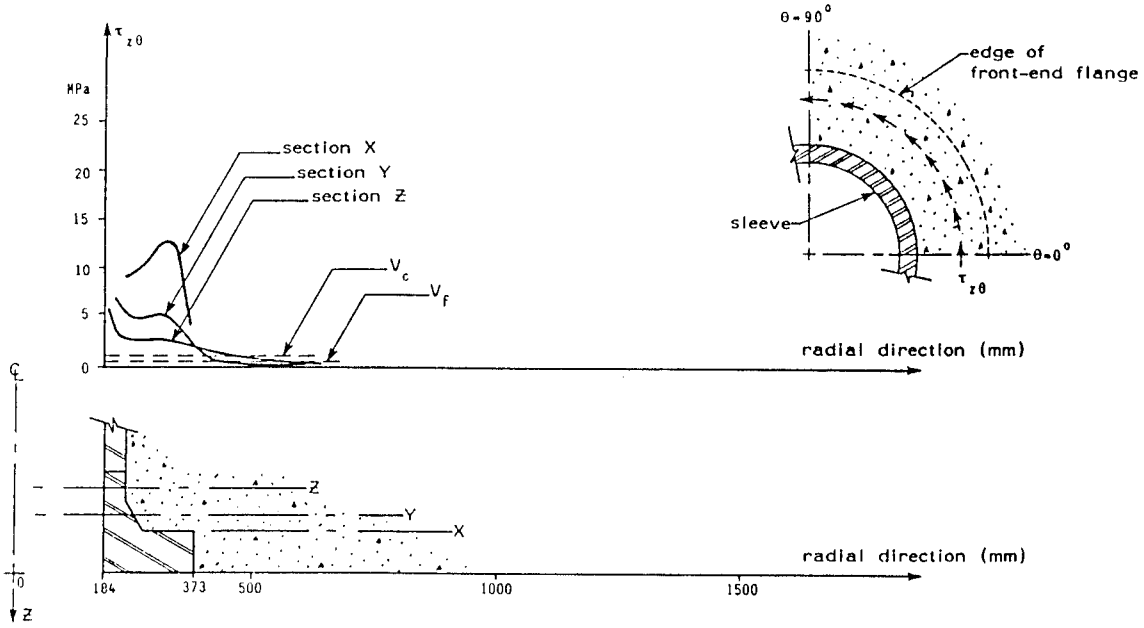

FIG. 17: TANGENTIAL SHEAR STRESS ($\tau_{z\theta}$) OF CONCRETE BEHIND THE FLANGE
LOAD CASE 4 = TORSION

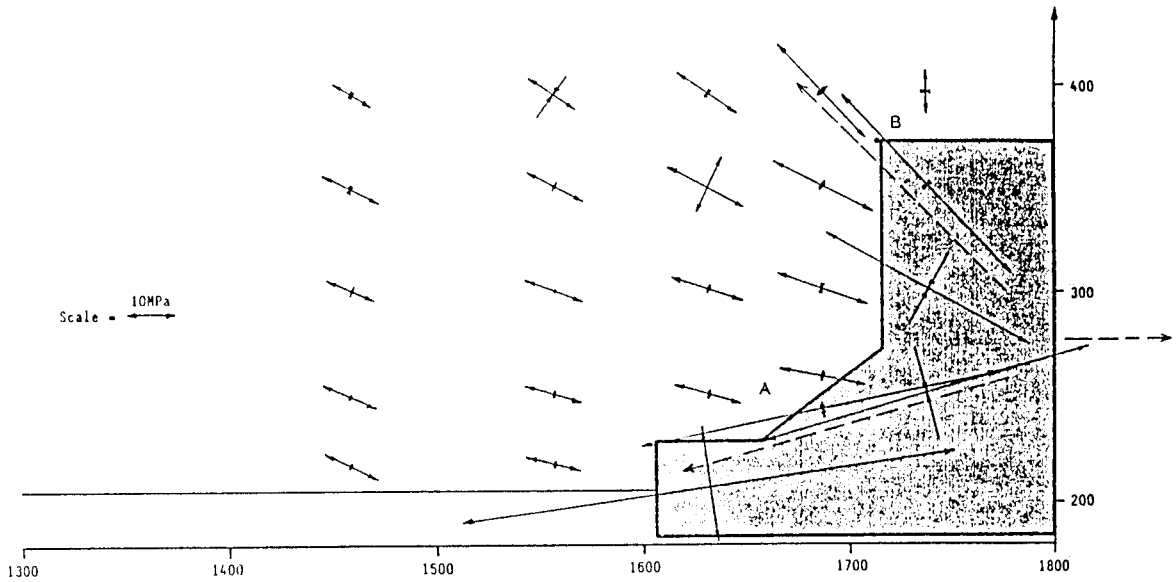

FIG. 18: VECTOR PLOT OF PRINCIPAL STRESSES
LOAD CASE 1 = AXIAL FORCE

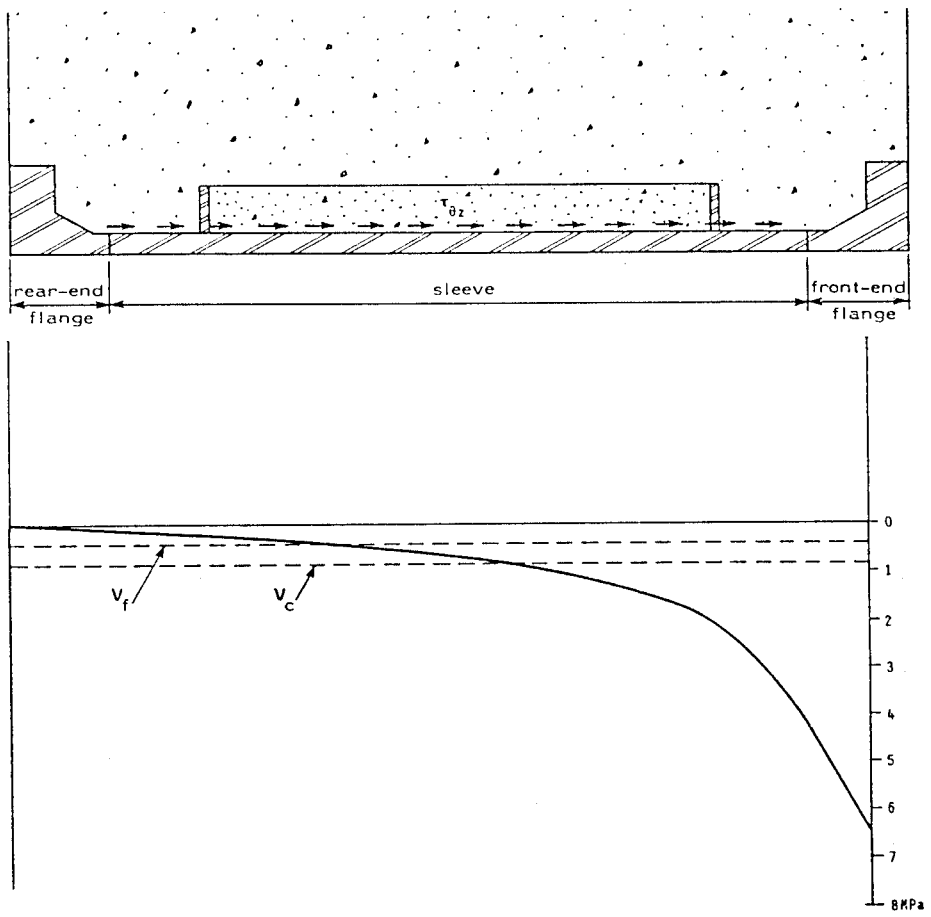

FIG. 19: TANGENTIAL SHEAR STRESS ($\tau_{\theta z}$) OF CONCRETE AT θ = 90°
LOAD CASE 3 = BENDING MOMENT

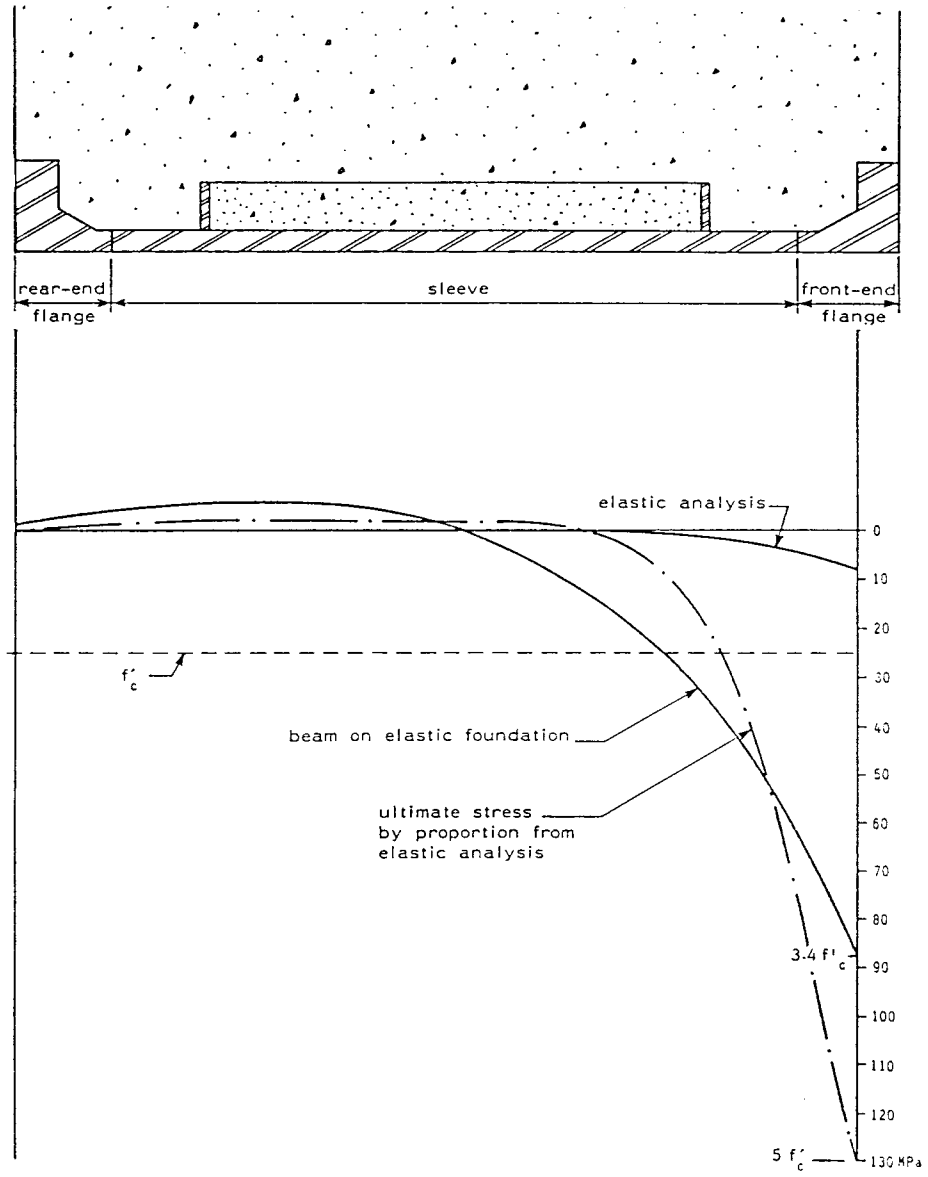

FIG. 20: RADIAL NORMAL STRESS (σ_r) OF CONCRETE AT θ = 90°
LOAD CASE 2 = SHEAR FORCE

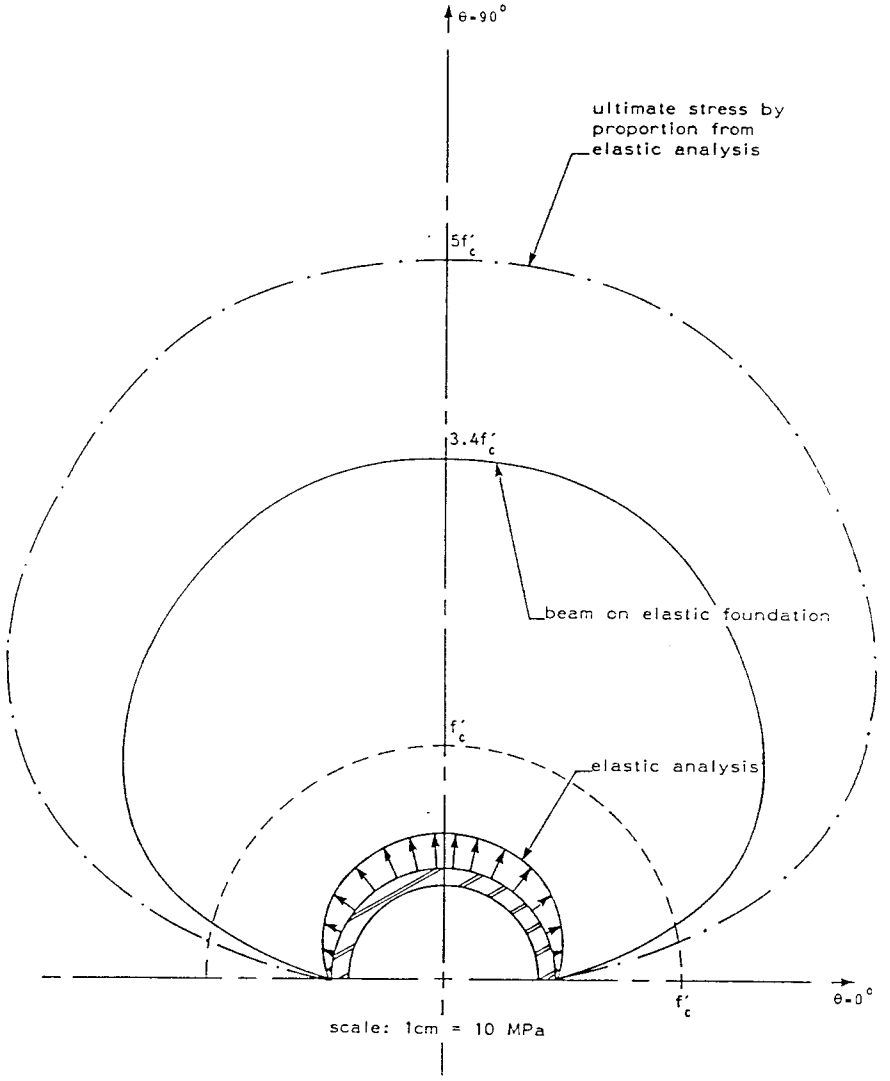

FIG. 21: RADIAL NORMAL STRESS (σ_r) OF CONCRETE BEHIND THE FLANGE
LOAD CASE 2 = SHEAR FORCE

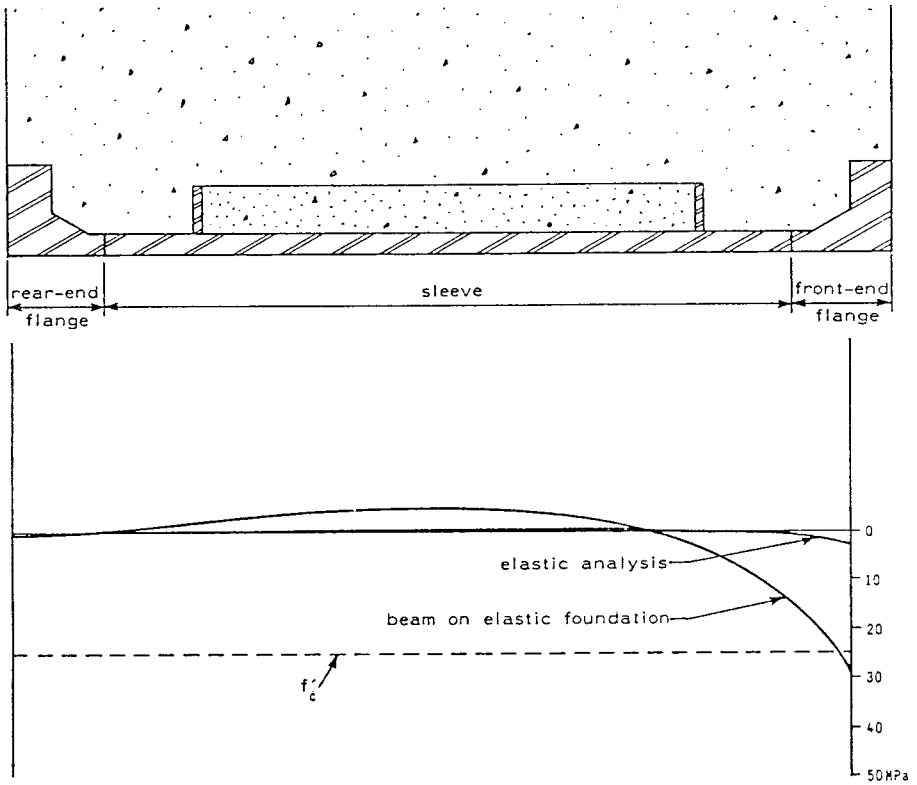

FIG. 22: RADIAL NORMAL STRESS (σ_r) OF CONCRETE AT θ = 0°
LOAD CASE 3 = BENDING MOMENT

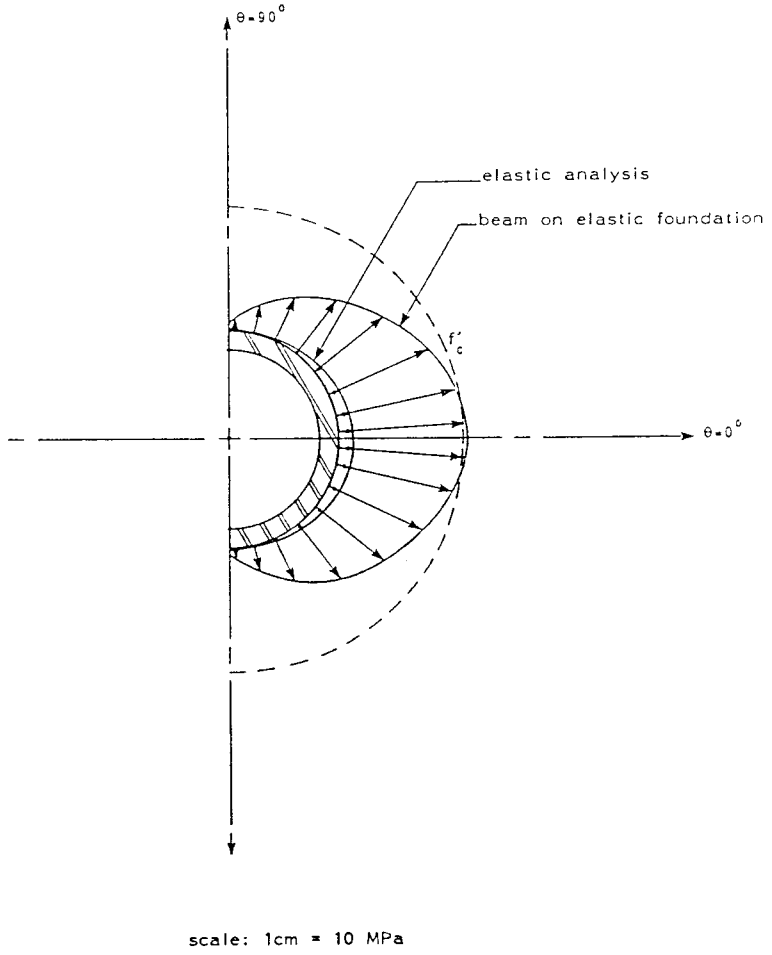

FIG. 23: RADIAL NORMAL STRESS (σ_r) OF CONCRETE BEHIND THE FLANGE
LOAD CASE 3 = BENDING MOMENT

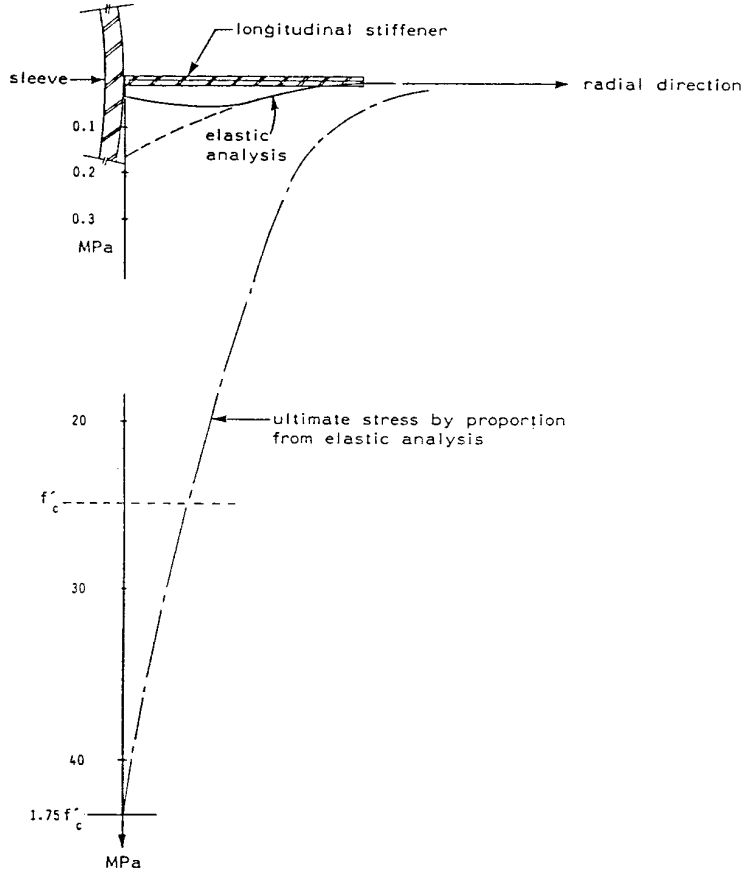

FIG. 24: BEARING STRESS (σ_θ) BETWEEN CONCRETE AND LONGITUDINAL STIFFENERS ALONG THE RADIAL DIRECTION
LOAD CASE 4 = TORSION

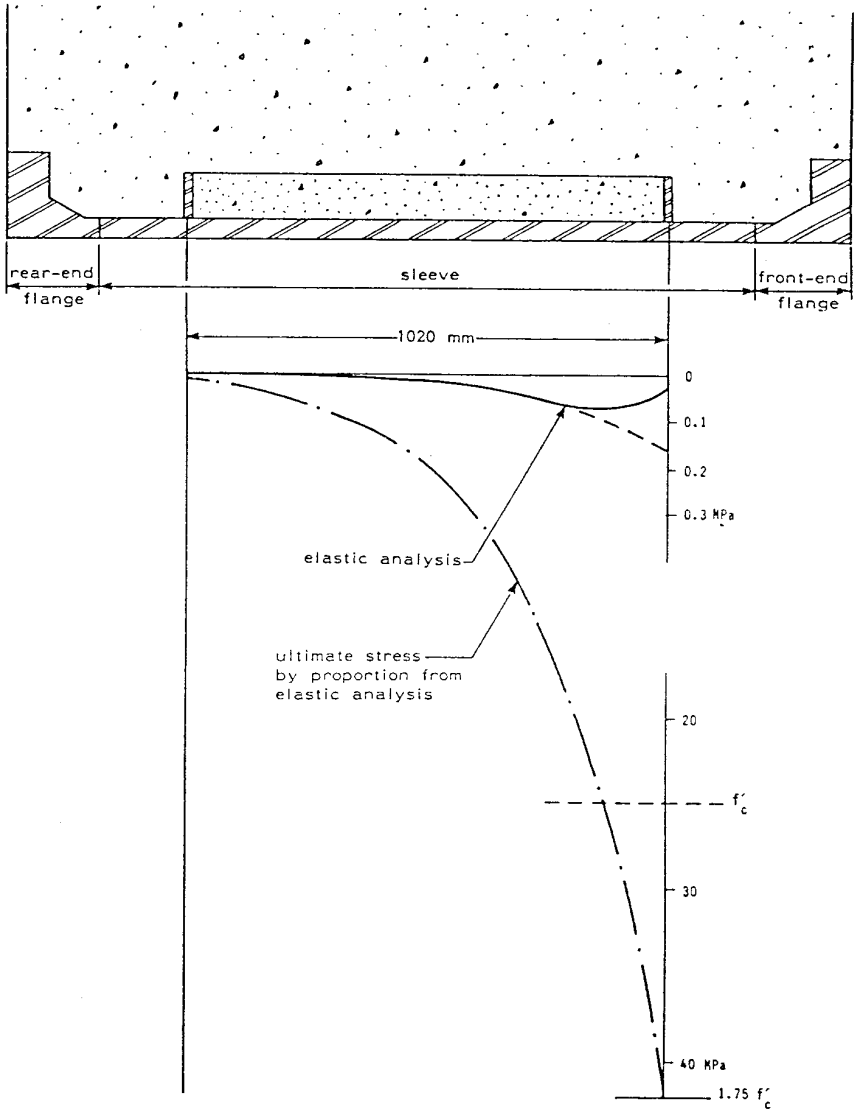

FIG. 25: BEARING STRESS (σ_θ) BETWEEN CONCRETE AND LONGITUDINAL STIFFENERS ALONG THE LONGITUDINAL DIRECTION
LOAD CASE 4 = TORSION